Observed suppression of ozone formation at extremely high temperatures due to chemical and biophysical feedbacks

Allison L. Steiner[a,1], Adam J. Davis[a], Sanford Sillman[a], Robert C. Owen[a], Anna M. Michalak[a,b], and Arlene M. Fiore[c]

[a]Department of Atmospheric, Oceanic and Space Sciences, University of Michigan, Ann Arbor, MI 48109; [b]Department of Civil and Environmental Engineering, University of Michigan, Ann Arbor, MI 48109; and [c]National Oceanic and Atmospheric Administration Geophysical Fluid Dynamics Laboratory, Princeton, NJ 08540

Edited by Barbara J. Finlayson-Pitts, University of California, Irvine, CA 92697, and approved September 24, 2010 (received for review June 15, 2010)

Ground level ozone concentrations ([O_3]) typically show a direct linear relationship with surface air temperature. Three decades of California measurements provide evidence of a statistically significant change in the ozone-temperature slope ($\Delta m_{O3\text{-}T}$) under extremely high temperatures (>312 K). This $\Delta m_{O3\text{-}T}$ leads to a plateau or decrease in [O_3], reflecting the diminished role of nitrogen oxide sequestration by peroxyacetyl nitrates and reduced biogenic isoprene emissions at high temperatures. Despite inclusion of these processes in global and regional chemistry-climate models, a statistically significant change in $\Delta m_{O3\text{-}T}$ has not been noted in prior studies. Future climate projections suggest a more frequent and spatially widespread occurrence of this $\Delta m_{O3\text{-}T}$ response, confounding predictions of extreme ozone events based on the historically observed linear relationship.

atmospheric chemistry | isoprene | meteorology | PAN

Temperature is often used as a predictor for high [O_3] (1, 2) because of its direct influence on chemical kinetic rates and the mechanism pathway for the generation of O_3 [e.g., H-abstraction versus OH addition (3)] and strong correlation with stagnant, sunny atmospheric conditions (4). [O_3] increases with temperature with a slope ($m_{O3\text{-}T}$) in the range of 2–8 ppb K^{-1} (4–10), and several studies have attempted to isolate the drivers of this relationship, as summarized in ref. 11. Early studies investigating the ozone-temperature relationship noted the impact of peroxyacetyl nitrate (PAN) decomposition on ozone formation (4, 12). The PAN sink for NO_x and odd hydrogen (HO_x) decreases exponentially as temperatures increase, implying a saturation of ozone formation from PAN decomposition as temperatures increase above ~310 K. Sillman and Samson (10) found that $m_{O3\text{-}T}$ is a function of multiple chemical processes, including the reaction rate of PAN, emissions of biogenic volatile organic compounds (VOC), photolysis rates, and water vapor concentrations. Therefore whereas absolute temperature is a strong predictor of the effects of incremental temperature change on ozone (2), chemical kinetics and temperature-dependent emission rates further complicate this relationship. For example, prior studies have noted that $m_{O3\text{-}T}$ varies between regions with different NO_x/VOC ratios (13), and can decrease following significant NO_x emissions reductions (6). The $m_{O3\text{-}T}$ relationship has been called a climate change "penalty," signifying that emissions reductions will need to be more stringent to counteract the effects of warming temperatures (6, 14). However, the stationarity of this ozone-temperature relationship has yet to be evaluated using observations over a broad range of temperatures.

High concentrations of tropospheric ozone ([O_3]) are an indicator of poor air quality, and adversely affect the health of humans and ecosystems (15, 16). A suite of chemical and meteorological factors contributes to the formation of ozone. Photochemically driven reactions of VOC in the presence of nitrogen oxides (NO_x) can form ozone at the surface (17), whereas stagnant meteorological conditions promote and maintain ozone events. Changes in the frequency of certain meteorological features such as fewer midlatitude cyclones (18, 19) or shallower boundary layer depths (20) can also increase [O_3]. Whereas significant progress has been made in understanding ozone formation from precursor emissions under varying meteorological and chemical conditions (17, 21), ozone formation under future climatic conditions is limited by model representations of emissions, atmospheric chemical processes, and meteorology (22, 23).

California provides a unique locale to evaluate the ozone-temperature relationship due to the relatively long ozone measurement record and the wide range of climatic zones leading to large variations in temperature across the state. Here we analyze the ozone-temperature relationship from 1980–2005 for four air basins in California: the Sacramento Valley, the San Joaquin Valley, the San Francisco Bay Area, and the South Coast air basins. We employ observations of ground-based ozone from a series of monitoring stations established by the California Air Resources Board (Fig. S1). Daily maximum surface air temperature (T_{max}) data are obtained from a statistically interpolated gridded product of ground-based National Oceanic and Atmospheric Administration (NOAA) station data at 1/8° resolution over the same time period (24). These [O_3] measurements provide a unique test-bed for the evaluation of $m_{O3\text{-}T}$ over a broader range of temperatures than considered by prior studies.

Results

Relationships between the daily 1 hour maximum [O_3] ($[O_3]_{max}$) and T_{max} from June 1-October 31 (reflecting the "ozone season" in California) are separated by air basin and decade (Fig. 1). The plateau of concentrations below 295 K suggests a background [O_3] of 30–40 ppb. From 295-312 K, $[O_3]_{max}$ increases approximately linearly with temperature with a slope ($m_{O3\text{-}T}$) of 2–8 ppb K^{-1}. In all air basins, $m_{O3\text{-}T}$ decreases over time reflecting a reduction in NO_x and VOC emissions from the 1980s to present, with changes in the South Coast the most dramatic and little change in the San Joaquin Valley. As temperatures increase above 312 K into an extremely high temperature range, conditions not unusual for the Central Valley of California, $[O_3]_{max}$ levels off and decreases slightly in some air basins and decades. To date, this response has been observed at other sites but a statistically significant relationship has yet to be determined (6, 9). The response is slightly different in each air basin due to varying precursor emissions and chemistry, yet the observed

Author contributions: A.L.S., A.M.M., and A.M.F. designed research; A.L.S. and A.J.D. performed research; S.S., R.C.O., and A.M.M. contributed new reagents/analytic tools; A.L.S., A.J.D., R.C.O., and A.M.M. analyzed data; and A.L.S., S.S., and A.M.F. wrote the paper.

The authors declare no conflict of interest.

This article is a PNAS Direct Submission.

[1]To whom correspondence should be addressed. E-mail: alsteiner@umich.edu.

This article contains supporting information online at www.pnas.org/lookup/suppl/doi:10.1073/pnas.1008336107/-/DCSupplemental.

ENVIRONMENTAL SCIENCES

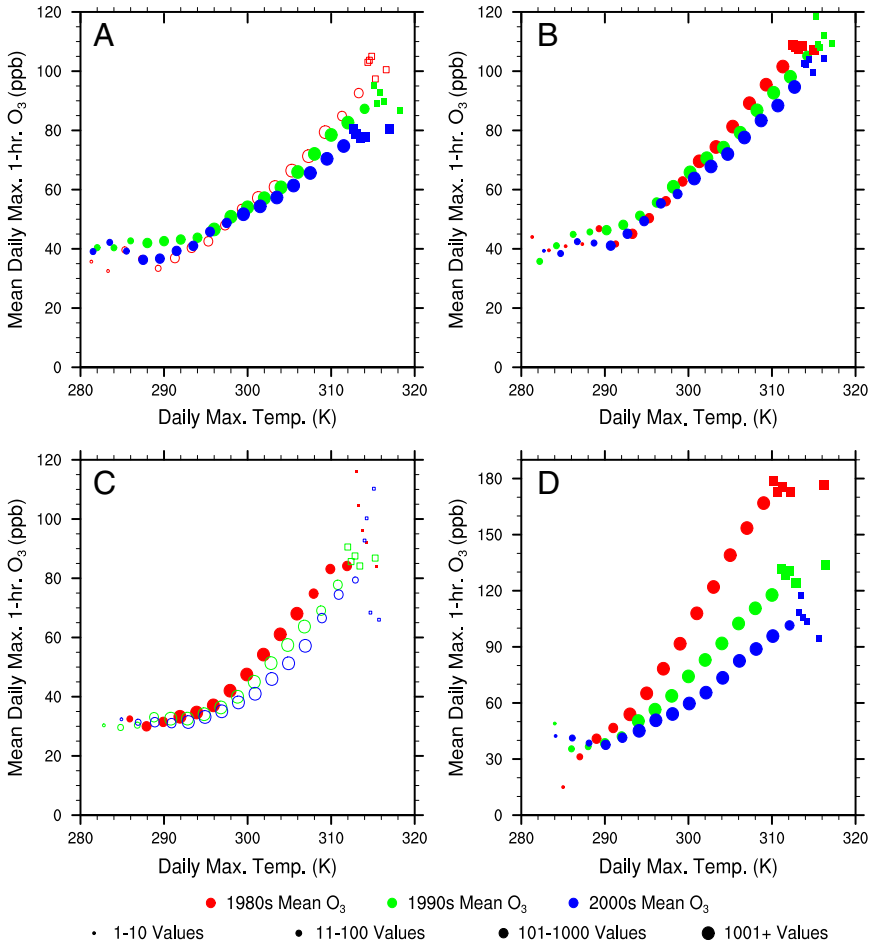

Fig. 1. Observed ozone–temperature relationships in California (1980–2005). Points represent the mean diurnal $[O_3]_{max}$ for all sites and days versus local maximum surface air temperature in (*A*) the Sacramento Valley air basin, (*B*) the San Joaquin Valley air basin, (*C*) the San Francisco Bay air basin, and (*d*) the South Coast air basin. Data below the high temperature cutoff are binned to 2 °K intervals (circles), whereas data above the temperature cutoff are binned into five bins each representing the average of one fifth of the observations above the high temperature cutoff (squares). Different binning above the high temperature cutoff displays the behavior of $[O_3]_{max}$ in the relatively narrow temperature range above the cutoff and corresponds with the linear regression statistics (Table 1). Results are shown for 1980–1989 (red), 1990–1999 (green), and 2000–2005 (blue). Symbol size indicates the number of data points in each bin. Filled symbols indicate a statistically significant decrease ($p < 0.05$) of $m_{O3\text{-}T}$ above the temperature cutoff [310–315 °K depending on basin and decade (Table 1)]; open symbols indicate the change was not significant.

$\Delta m_{O3\text{-}T}$ is consistent across decade, air basin, and individual stations. This high-temperature ozone response ($\Delta m_{O3\text{-}T}$) is statistically significant ($p < 0.05$; Fig. 1 and Table 1) for all response curves except Sacramento in the 1980s and San Francisco in the 1990s and 2000s. The lack of significance for these particular basins and decades is likely due to the low number of ozone observations in this temperature range. Additionally, $\Delta m_{O3\text{-}T}$ is consistent across five different percentiles of the ozone distribution, suggesting that the high-temperature response is not dependent on the value of $[O_3]_{max}$. To understand the behavior of $m_{O3\text{-}T}$ at these extremely hot temperatures, we evaluate two possible factors: (*i*) changes in the emissions of ozone precursors and their influence on the chemical formation, or (*ii*) changes in the large-scale meteorological conditions at extremely high temperatures.

To evaluate changes in precursors and their role in ozone production, we use a photochemical box model for two Central Valley locations (Sacramento and Fresno). Sacramento represents a VOC-limited ozone formation regime and Fresno is roughly between the VOC-limited and NO_x-limited regimes (13), allowing the results to span a range of VOC and NO_x limitation. The base case simulations for each location calculate photochemistry for a 2 day period using urban emissions estimates. In the base case, $[O_3]_{max}$ increases with increasing T_{max} and plateaus at approximately 316 K (Fig. 2*A* and *B*). An analysis of chemical destruction and loss indicates that this plateau is predominantly caused by PAN chemistry. At low temperatures, net formation of PAN (coincident with the formation of ozone) represents a significant net sink for both NO_x and HO_x. Thermal decomposition of PAN

Table 1. Statistical analysis parameters for the ozone-temperature evaluation

Air basin	Decade	T_{max} cutoff (K)	*p* value	$m_{O3\text{-}T}{}^{N}$ 295–310 K (ppb K^{-1})	$m_{O3\text{-}T}{}^{H}$ above cutoff (ppb K^{-1})
Sacramento Valley	1980s	314.3	1.5e−1	2.496	−0.951
	1990s	315.0	3.7e−4	2.232	−2.399
	2000s	312.5	1.3e−2	1.806	0.399
San Joaquin Valley	1980s	312.3	2.52e−4	3.276	−0.285
	1990s	315.2	7.8e−3	2.579	−1.842
	2000s	313.7	1.3e−2	2.410	0.423
San Francisco Bay	1980s	312.9	2.6e−2	3.179	−9.071
	1990s	311.8	5.3e−2	2.673	−0.776
	2000s	313.9	7.0e−2	2.277	−7.776
South Coast	1980s	310.0	3.2e−5	7.603	0.171
	1990s	311.0	3.8e−3	4.638	0.847
	2000s	313.1	3.4e−14	3.388	−8.527

T_{max} cutoff values and slopes ($m_{O3\text{-}T}{}^{N}$ and $m_{O3\text{-}T}{}^{H}$) are determined using all available individual observations (i.e., raw data), and therefore the calculated slopes may vary visually from those seen in the binned data displayed in Fig. 1. Bold values indicate that the relationship is statistically significant using a criterion of $p < 0.05$.

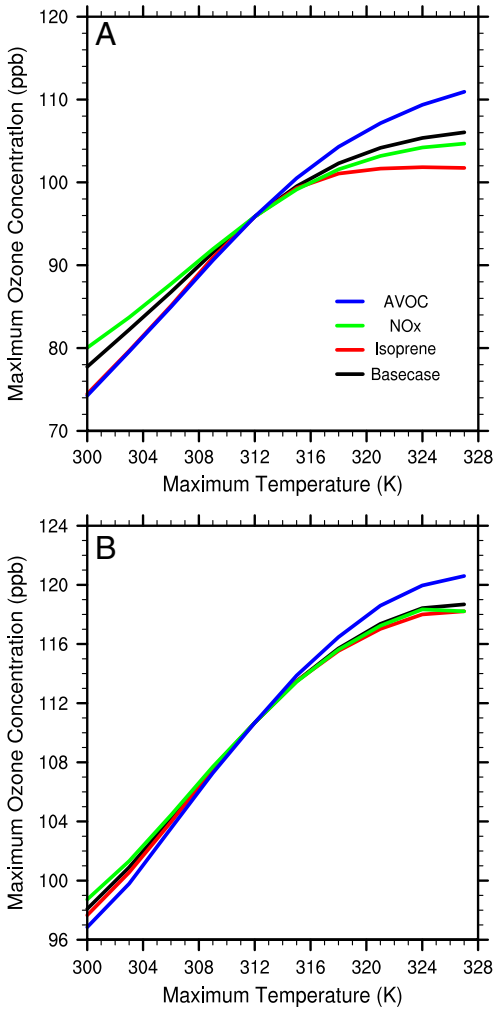

Fig. 2. Modeled ozone–temperature relationships. Simulations in (*A*) Sacramento and (*B*) Fresno for present-day emissions and concentrations (black) and three emissions sensitivity tests: NO_x-dependent emissions (green), anthropogenic VOC-temperature dependent emissions (blue), and isoprene emissions as a function of temperature (increasing to 310 K and decreasing thereafter; red).

becomes more rapid as temperatures increase, confining less NO_x and HO_x in PAN and causing an increase in $[O_3]_{max}$ with warmer T_{max}. However, the impact of further temperature increases diminishes at temperatures above approximately 312 K. The PAN lifetime decreases at an e-folding rate every 6.5 K (or approximately halving every 4.5 K in the range of 280–320 K), leading to a similar decrease in the net PAN sink. Above 312 K, the effect of further changes in the PAN lifetime has less effect on chemistry, leading to a plateau in $[O_3]_{max}$.

Whereas the PAN decomposition rate can explain a plateau in $[O_3]_{max}$, it cannot explain the observed decrease in $[O_3]_{max}$ in some locations. Additional emission scenarios are modeled to account for changes in ozone precursor emissions with temperature, where emission rate changes are scaled to the temperature in the base case scenario of 313 K. Although anthropogenic NO_x emissions will likely increase as a result of increased energy demand [estimated to be approximately 1200 MW K^{-1} (25)], much of the state's electricity is generated out of state during peak demand periods (26), which results in a highly uncertain link between local NO_x emissions and warmer temperatures. However, anthropogenic VOC emissions (e.g., evaporative emissions, industrial processes) are local and affected by warmer temperatures. Three sensitivity tests include (*i*) NO_x: warmer temperatures increase energy demand and increase NO_x (1% increase per 3 K, reflecting a similar rate as anthropogenic VOC emissions and representing a conservative estimate due to out-of-state emissions), (*ii*) AVOC: an increase in anthropogenic VOC emissions due to a rise in evaporative emissions [1% increase per 3 K; (27)], and (*iii*) Isoprene: a temperature-dependent change in isoprene emissions, where isoprene emissions increase with temperature until approximately 310 K then decrease due to biophysical high-temperature constraints (28). Isoprene emissions are known decrease under drought conditions (29), exhibit strong interspecies variability, and have been observed to acclimate to various temperature maxima (30). As a result, large variability in the temperature at which isoprene decreases is expected, and here we employ the standard isoprene-temperature parameterization based on Guenther et al. (28) to determine the plausibility of this biogenic feedback.

In both Sacramento and Fresno, NO_x and VOC sensitivity tests show the sign and magnitude of $\Delta m_{O3\text{-}T}$ depends on the relative degree of VOC or NO_x sensitivity. Sacramento is slightly NO_x-sensitive and strongly VOC-sensitive, whereas Fresno is less NO_x-sensitive and slightly VOC-sensitive. Due to stronger VOC sensitivity, the Sacramento case exhibits a slight decrease in $[O_3]_{max}$ at high temperatures due to temperature-sensitive isoprene emissions. This suggests that the temperature dependence of isoprene emissions could be responsible for the observed ozone decrease (Fig. 1). We evaluate observed isoprene concentrations as a function of temperature and find that isoprene increases with increasing temperatures in the range of 290–312 K and decreases with further temperature increases, a pattern of temperature dependence comparable to observed ozone (Fig. 3). Although the Sacramento data do not have measurements in the extremely high temperature range, isoprene concentrations in the San Joaquin and South Coast air basins decrease above 312 K. Together, the model and observations suggest reductions in isoprene emissions could be responsible for the observed decrease in ozone at extremely high temperatures.

Meteorological features can also influence ozone production through changes in convective activity, mesoscale circulation, and boundary layer height. Convective activity and precipitation can limit ozone production in other regions in the United States; however, we note that convective precipitation is nearly absent during California due to the dry summer conditions and we exclude this possibility. We focus on two regional meteorological features that could lead to $\Delta m_{O3\text{-}T}$, including the land-sea breeze circulation and changes in the boundary layer height.

The land-sea breeze plays a key role in boundary layer circulation and temperatures in the California region during the dry summers in California (31). Mesoscale flow in central California is driven by heating in the continental interior, causing air to rise and drawing in cleaner air from the Pacific marine boundary layer. Extremely high temperature conditions could enhance this circulation, increasing wind speeds into the Central Valley and diluting ozone. To determine if the general circulation pattern changes under extremely high temperatures, we conduct a series of Hybrid Single Particle Lagrangian Integrated Trajectory Model (HYSPLIT) back-trajectory analyses for Sacramento and Fresno (*SI Text*). Back-trajectory analyses are binned by T_{max} into moderately hot days (306 K $\leq T_{max} \leq$ 310 K; 1148 trajectories in Sacramento and 606 trajectories in Fresno) and extremely hot days ($T_{max} \geq$ 312 K; 258 trajectories in Sacramento and 147 trajectories in Fresno), and a cluster analysis is performed to determine the dominant circulation patterns (Fig. S2). For Sacramento, onshore flow (defined as air moving from ocean to land) accounts for about 90% of the flow in the moderate temperature case. In the high-temperature case, 73% of the flow is onshore, with an additional 20% of the trajectories indicating valley recirculation. For Fresno, onshore flow accounts for approximately 95% of the trajectories in both cases, yet trajectories

ENVIRONMENTAL SCIENCES

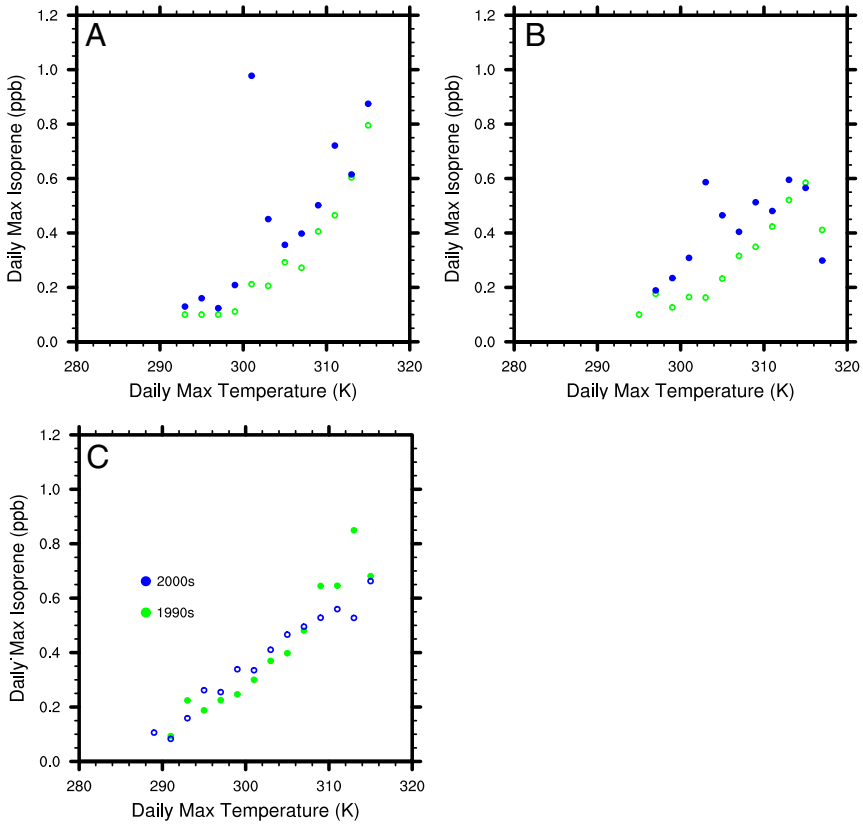

Fig. 3. Observed isoprene-temperature relationships. EPA PAMS isoprene concentrations from 1993–2005 for (*A*) the Sacramento, (*B*) the San Joaquin, and (*C*) the South Coast air basins (locations in Fig. S1). Filled circles indicate a statistically significant decrease ($p < 0.05$) of the isoprene-temperature slope; open circles indicate that the change was not significant.

in the high-temperature case indicate slower wind speeds and greater stagnation in the Valley. Overall, the results from the cluster analysis do not suggest a strengthened land-sea breeze circulation and are instead more indicative of slower wind speeds and stagnation on extremely hot days. Therefore, increased cleaner air from onshore flow is not a likely cause of reduced $[O_3]_{max}$ at high temperatures and in fact indicates circulation changes may cause $[O_3]_{max}$ to increase on extremely hot days.

A second meteorological phenomenon that could explain $\Delta m_{O3,T}$ is an increase in the atmospheric boundary layer (ABL) height. Extremely high temperatures could increase surface heat fluxes and convective mixing, thereby increasing the ABL height and diluting ozone concentrations. ABL heights in the summertime in Central California typically range from 1–2 km due to the presence of persistent high pressure systems aloft, creating strong subsidence and preventing the ABL height from growing with surface temperatures (32). Concurrent ozone and ABL height observations were not available in Central Valley, therefore we analyze a limited dataset of ABL height soundings from 2007–2009 (*SI Text*). The number of extremely high-temperature days for this three-year analysis is too limited for statistical significance testing, yet does not suggest higher ABLs under extremely hot temperature regimes. In fact, observed ABL heights for the extremely high-temperature days are often lower than ABL heights under moderate temperatures (Fig. S3), suggesting that ABL height is not a driving factor in $\Delta m_{O3\text{-}T}$. As a result, we conclude that $\Delta m_{O3\text{-}T}$ is driven by atmospheric chemistry and ecosystem-climate interactions.

Discussion

Presently, daily $T_{max} > 312$ K occur at limited locations throughout the continental United States, including 10–50 days yr^{-1} in California's Central Valley, Texas, and the southern Great Plains, and 50–100 days yr^{-1} in the southwest (Fig. 4*A*). However, $\Delta m_{O3,T}$ may be increasingly important under warming climate scenarios. To evaluate changes under a future climate, we utilize climate projections from the North American Regional Climate Change Assessment Program (NARCCAP) (33). NARCCAP simulations are dynamically downscaled regional climate model simulations forced by general circulation models implementing the Special Report on Emissions Scenarios A2 greenhouse gas concentrations for the 21st century. Estimates of near-term future climate (2041–2065) indicate a range of climate responses, shown here representing a relatively high estimate (Fig. 4*B*) and a relatively conservative estimate (Fig. 4*C*) of T_{max}. In both cases, the spatial extent affected by temperatures ≥312 K increases to encompass about 50–75% of land area in the continental United States. In Texas and the southeast, regions with historical violations of federal ozone standards, $[O_3]_{max}$ plateau or decrease 20–100 days yr^{-1}. Regions with strong isoprene sources and NO_x sources where chemistry is more VOC-limited could experience a decrease in $[O_3]_{max}$ at extremely high temperatures.

Observations in California provide compelling evidence that $[O_3]_{max}$ may plateau or decrease under extremely high temperatures (>312 K). This response is a strong function of an e-folding decrease of PAN and a reduction of isoprene emissions at these high temperatures. Whereas these chemistry responses are known and included in some atmospheric chemistry models, the results presented here represent statistically significant evidence of this change in observed or modeled $m_{O3\text{-}T}$. Additionally, this work suggests that using purely meteorological drivers to extrapolate the effects of future climate on air quality is insufficient, and only models that can capture the complex nature of the PAN chemistry and biogenic VOC emissions will be able to assess these effects accurately. These results indicate that chemical and biophysical feedbacks may slow ozone formation at extremely high temperature conditions, but we note that this response is not equivalent to assuming that warmer climates will result in improved air quality. In fact, seasonal studies indicate that the ozone season is already lengthening as the climate warms (34). The phenomenon presented here highlights the complexity of biosphere–chemistry–climate interactions, and we suggest that

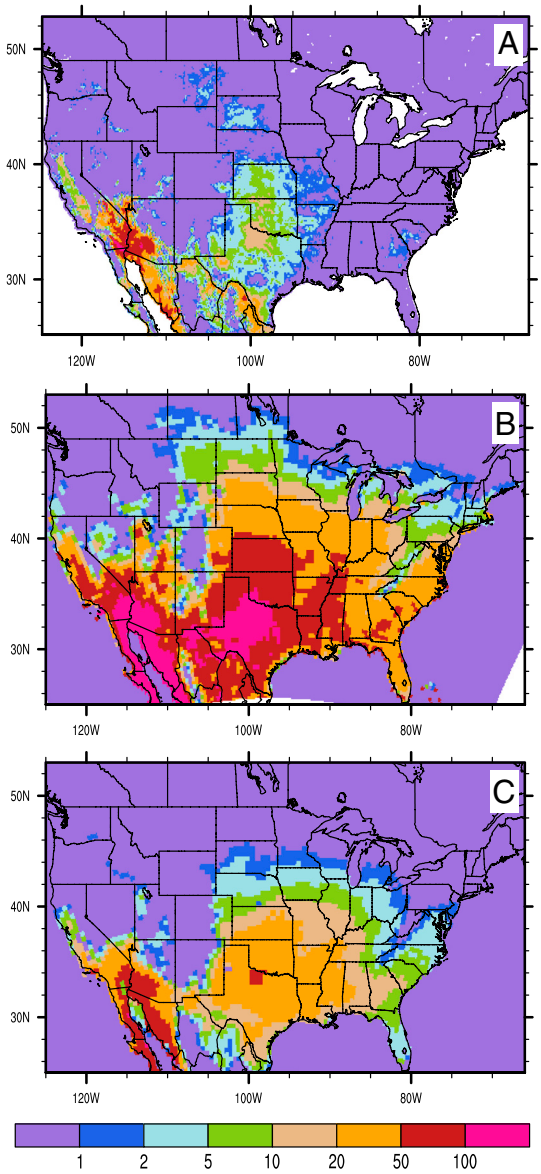

Fig. 4. (*A*) Present day average number of days per year with temperatures ≥312 K (1980–2000; ref. 23). Potential average number of days per year ≥312 K based on two NARCCAP future climate realizations (29), indicating (*B*) a substantial increase in future climate daily T_{max} (CRM-CGCM) and (*C*) a conservative increase in future climate daily T_{max} (RCM-GFDL).

this feedback be included in future estimates of $\Delta m_{O3\text{-}T}$ and the climate change penalty incurred on ozone precursor emissions reductions.

Materials and Methods

Ozone Data. We employ observations of ground-based ozone from a series of monitoring stations established by the California Air Resources Board [CARB (35)] from 1980–2005 (Fig. S1). We focus on locations in four air basins in California: the Sacramento Valley, the San Joaquin Valley, the San Francisco Bay Area, and the South Coast. In the past decade, the Central Valley (encompassing the Sacramento and San Joaquin Valleys) and the South Coast air basins typically exceed the 1 hour state ozone standard approximately 50–100 times per year, and exceed the 8 hour federal standard 50–120 times per year (36). The San Francisco Bay air basin has fewer violations (usually 10–20 exceedances of the 1 hour state standard and less than 20 violations of the 8 hour federal standard), yet is a large source of ozone precursor emissions to the Central Valley sites. We utilize data from up to 22, 19, 28, and 22 CARB and district sites in the Sacramento, San Joaquin, South Coast, and San Francisco Bay air basins, respectively, over approximately three decades. At the CARB and district sites, ozone is sampled on a continuous hourly basis using ultraviolet photometry.

Temperature Data. We utilize daily maximum surface air temperature from the 1/8th degree gridded dataset by Maurer et al. (24). The stations used in this analysis are predominantly from the NOAA Cooperative Observer stations, with an average station density of one station per 700 km^2 over the entire United States (24). Gridded data is available through 2005, therefore data analysis in the 2000s decade is limited by the available meteorological data.

Isoprene Concentration Data. Isoprene concentration data is obtained from the Environmental Protection Agency (EPA) Photochemical Assessment Monitoring Stations (PAMS) (www.epa.gov/air/oaqps/pams). Isoprene monitoring locations are noted in Fig. S1. Data is available for 21 sites in three air basins in 1993–2005, including four sites in the Sacramento Valley, nine sites in the San Joaquin Valley, and eight sites in the South Coast air basin.

Statistical Significance. Statistical significance testing for the ozone-temperature slope change ($\Delta m_{O3\text{-}T}$) uses a one-tailed Z test to evaluate if the computed linear slope within an "extremely high" temperature regime is significantly less than the linear slope within a "normal" temperature regime, at a 95% confidence level ($\alpha = 0.05$). Daily maximum ozone and daily maximum temperature data are segregated into two sets, one including all data with a temperature greater than 295 K and less than a high-temperature cutoff (the normal temperature regime), and the other including all data with a temperature greater than or equal to the high-temperature cutoff (the extremely high temperature regime). An ordinary least-squares linear regression is performed on the raw (i.e., not temperature-binned) data for each set, using temperature as the independent variable and ozone as the dependent variable (Table 1).

A Z test statistic determines if the slope at extremely high temperatures is significantly lower than at normal temperatures:

$$Z = \frac{(m_{O3,T}{}^{H} - m_{O3,T}{}^{N}) - 0}{\sqrt{\frac{\sigma^2_H}{n_H} + \frac{\sigma^2_N}{n_N}}}$$

where H superscripts and subscripts denote the extremely high temperature regime and N superscripts and subscripts refer to the normal temperature regime. $m_{O3,T}$ represents the ozone-temperature slope (values in Table 1), σ^2 is the variance of regression residuals, and n represents the number of data points in the given subset. Note that the statistical significance of the slope difference can also be calculated by isolating the difference in slope above the temperature cutoff directly, but the above approach has the advantage of allowing for different residual variances above and below the cutoff. Because the residuals for extremely high temperatures have a higher variance than those at lower temperatures, the above method was selected although the conclusions regarding the significance of the slope difference were largely consistent for both approaches.

The statistical significance is expressed as the p-value for the computed test statistic Z (Table 1), representing the probability that the reduction in slope is due to random sampling variability rather than a true difference in behavior. The p-value for a lower-bound hypothesis test is calculated as the cumulative probability of a standard normal distribution up to the computed value of Z. A p-value below 0.05 implies a significant reduction in slope at the $\alpha = 0.05$ significance level.

The high-temperature cutoff value for each air basin and decade, which is used to segregate the ozone-temperature data pairs into the normal and extremely hot temperature regimes, is chosen to maximize the significance of the difference in slope. Ultimately, the cutoff temperature (noted in Table 1) that is used for each dataset is the one that results in the most significantly different slope between the normal temperature and the extremely high temperature slopes. A similar statistical analysis was performed for the isoprene-temperature relationship (Fig. 3) with statistics presented in Table S1.

Photochemical Box Model Simulations. The box model [with modifications described in (37)] calculates urban photochemistry for a single grid cell. Ambient concentrations are continually diluted by horizontal advection (based on a 1.5 m s^{-1} wind) and entrainment from aloft (with mixing height increasing from 150 m at night to 1500 m in the afternoon). Temperature varies diurnally over a range of 20 K, which is typical for California's Central Valley (32). Photochemistry is based on the GEOS-Chem mechanism (38) with extensions for urban photochemistry (39). Initial, upwind and aloft primary VOC and NO_x concentrations are set equal to 24 hour average values from 3D air quality simulations described in Steiner et al. (13). Emission rates for Sacra-

ENVIRONMENTAL SCIENCES

mento and Fresno are derived from regional air quality simulations and based on a maximum local temperature of 313 K (13). Initial, upwind and aloft $[O_3]$ are set to background values (40 ppb) to avoid inclusion of O_3 associated with local or regional production. Separate simulations are conducted for each temperature bin, and the diurnal T_{max} is plotted versus $[O_3]_{max}$ in Fig. 3.

We note that the range of modeled $[O_3]_{max}$ and $m_{O3\text{-}T}$ differs from observed values. For example, observed and modeled $[O_3]_{max}$ are comparable at high temperatures (100–120 ppb in Sacramento and Fresno) yet over estimated at lower temperatures. Additionally, modeled $m_{O3\text{-}T}$ (1–1.5 ppb K^{-1}) is lower than that observed (2–3 ppb K^{-1}). This mismatch between observed and modeled $m_{O3\text{-}T}$ has been noted in other modeling studies (e.g., ref. 10), whereas Jacob et al. (4) found that approximately half the observed $m_{O3\text{-}T}$ can be explained by the association of high temperatures with stagnant dynamical conditions. Our meteorological analysis confirms this association for California. Additional evidence is found in the Ito et al. study (8), which reported a modeled $m_{O3\text{-}T}$ of 2–2.5 ppb K^{-1} for the Sierra foothills region of California and is comparable to observed $m_{O3\text{-}T}$ (40). Because Ito et al. (8) used the same chemistry as in the calculation shown here, it is plausible to attribute the difference in modeled and observed $m_{O3\text{-}T}$ to differences in dynamics, time of year and the occurrence of clouds or fog.

NARCCAP Future Climate Simulations. Future climate daily T_{max} are evaluated using dynamically downscaled simulations from the NARCCAP (33). Presently, the NARCCAP archives include four different future climate model simulations of the A2 emissions scenario for the time period of 2038–2070. To remove any effects of model spinup, we remove the first three years of this study for our analysis. Additionally, simulations through 2070 were not available for all regional models, therefore we analyze years 2041–2065 here. Three different regional climate models and varying global boundary conditions are available, including (*i*) Canadian Regional Climate Model (Fig. 4*A*) driven by the Canadian Global Climate Model version 3 (CGCM); (*ii*) the Hadley Center Regional Climate Model driven by the United Kingdom Hadley Centre Climate Model version 3 (HadCM3 resolution), (*iii*) the ICTP Regional Climate Model (RCM3) driven with the CGCM3, and (*iv*) RCM3 driven by the NOAA Geophysical Fluid Dynamics Laboratory Climate Model version 2.1(GFDL CM2.1) (Fig. 4*B*). The equilibrium climate sensitivities of the four driving boundary conditions are 3.4 °C (CGCM3), 2.7 °C (CCSM3), 3.4 °C (GFDL), and 3.3 °C (HadCM3); these simulations are centered on the middle of the Intergovernmental Panel on Climate Change sensitivity range of 2.1–4.4 °C and are close to the estimate of the most likely sensitivity range of 3.0 °C (41). For the figures presented in the main text of the paper, we select the most sensitive (CRM-CGCM3) and the least sensitive (RCM3-GFDL) of these options with respect to the spatial coverage and magnitude of daily T_{max} (Fig. 4).

ACKNOWLEDGMENTS. We thank Frank Marsik and Sharon Zhong for helpful comments and suggestions on this work. We acknowledge the use of the CARB ozone data and the EPA PAMS isoprene data. We thank the Naval Postgraduate Research Laboratory for the use of boundary layer height data, and the NOAA Air Resources Laboratory for the provision of the HYSPLIT transport and dispersion model. We thank NARCCAP for providing the future climate simulations (funded by the National Science Foundation, the US Department of Energy, NOAA, and the EPA). S.S. was supported by the Environmental Protection Agency to Achieve Results Program Grant RD-83337701-0.

1. Vukovich FM, Sherwell J (2003) An examination of the relationship between certain meteorological parameters and surface ozone variations in the Baltimore–Washington corridor. *Atmos Environ* 37:971–981.
2. Wise EK (2009) Climate-based sensitivity of air quality to climate change scenarios for the southwestern United States. *Int J Climatol* 29(1):87–97.
3. Atkinson R (1990) Gas-phase tropospheric chemistry of organic compounds: A review. *Atmos Environ* 24A:1–41.
4. Jacob DJ, et al. (1993) Simulation of summertime ozone over North America. *J Geophys Res-Atmos* 98(D8):14797–14816.
5. Aw J, Kleeman MJ (2003) Evaluating the first-order effect of intraannual temperature variability on urban air pollution. *J Geophys Res-Atmos* 108(D12):4365 10.1029/2002JD002688.
6. Bloomer BJ, Stehr JW, Piety CA, Salawitch RJ, Dickerson RR (2009) Observed relationships of ozone air pollution with temperature and emissions. *Geophys Res Lett* 36: L09803 10.1029/2009GL037308.
7. Camalier L, Cox W, Dolwick P (2007) The effects of meteorology on ozone in urban areas and their use in assessing ozone trends. *Atmos Environ* 41(33):7127–7137.
8. Ito A, Sillman S, Penner JE (2009) Global chemical transport model study of ozone response to changes in chemical kinetics and biogenic volatile organic compounds emissions due to increasing temperatures: Sensitivities to isoprene nitrate chemistry and grid resolution. *J Geophys Res-Atmos* 114 10.1029/2008JD011254.
9. Mahmud A, Tyree M, Cayan D, Motallebi N, Kleeman MJ (2008) Statistical downscaling of climate change impacts on ozone concentrations in California. *J Geophys Res-Atmos* 113 10.1029/2007JD009534.
10. Sillman S, Samson FJ (1995) Impact of temperature on oxidant photochemistry in urban, polluted, rural and remote environments. *J Geophys Res-Atmos* 100(D6): 11497–11508.
11. US Environmental Protection Agency (2005) *Air Quality Criteria for Ozone and Related Photochemical Oxidants* (National Center for the Environmental Assessment, Research Triangle Park, NC).
12. Cardelino CA, Chameides WL (1995) An observation-based model for analyzing ozone precursor relationships in the urban atmosphere. *J Air Waste Manage* 45(3):161–180.
13. Steiner AL, Tonse S, Cohen RC, Goldstein AH, Harley RA (2006) Influence of future climate and emissions on regional air quality in California. *J Geophys Res-Atmos* 111:D18303 10.1029/2005JD006935.
14. Wu SL, Mickley LJ, Jacob DJ, Rind D, Streets DG (2008) Effects of 2000–2050 changes in climate and emissions on global tropospheric ozone and the policy-relevant background surface ozone in the United States. *J Geophys Res-Atmos* 113:D06302 10.1029/2007JD008917.
15. Cape JN (2008) Surface ozone concentrations and ecosystem health: Past trends and a guide to future projections. *Sci Total Environ* 400(1–3):257–269.
16. Ebi KL, McGregor G (2008) Climate change, tropospheric ozone and particulate matter, and health impacts. *Environ Health Perspect* 116(11):1449–1455.
17. Sillman S (2003) Photochemical smog: ozone and its precursors. *Handbook of Weather, Climate, and Water*, eds T Potter and C BR (Wiley, New York), pp 227–242.
18. Leibensperger EM, Mickley LJ, Jacob DJ (2008) Sensitivity of US air quality to mid-latitude cyclone frequency and implications of 1980–2006 climate change. *Atmos Chem Phys* 8(23):7075–7086.
19. Mickley LJ, Jacob DJ, Field BD, Rind D (2004) Effects of future climate change on regional air pollution episodes in the United States. *Geophys Res Lett* 31:L24103 10.1029/2004GL021216.
20. Rao ST, Ku JY, Berman S, Zhang KS, Mao HT (2003) Summertime characteristics of the atmospheric boundary layer and relationships to ozone levels over the eastern United States. *Pure Appl Geophys* 160(1–2):21–55.
21. National Research Council (1991) *Rethinking the Ozone Problem in Rural and Regional Air Pollution* (National Academy Press, Washington, DC).
22. Jacob DJ, Winner DA (2009) Effect of climate change on air quality. *Atmos Environ* 43(1):51–63.
23. Weaver CP, et al. (2009) A preliminary synthesis of modeled climate change impacts on US regional ozone concentrations. *B Am Meteorol Soc* 90(12):1843–1863.
24. Maurer EP, Wood AW, Adam JC, Lettenmaier DP, Nijssen B (2002) A long-term hydrologically based dataset of land surface fluxes and states for the conterminous United States. *J Climate* 15(22):3237–3251.
25. Franco G, Sanstad AH (2008) Climate change and electricity demand in California. *Climatic Change* 87:139–151.
26. Miller N, Hayhoe K, Jin J, Auffhammer M (2008) Climate, extreme heat, and electricity demand in California. *J Appl Meteorol Clim* 47:1834–1844.
27. Rubin JI, Kean AJ, Harley RA, Millet DB, Goldstein AH (2006) Temperature dependence of volatile organic compound evaporative emissions from motor vehicles. *J Geophys Res-Atmos* 111 10.1029/2005JD006458.
28. Guenther AB, Zimmerman PR, Harley PC, Monson RK, Fall R (1993) Isoprene and monoterpene emission rate variability—Model evaluations and sensitivity analyses. *J Geophys Res-Atmos* 98(D7):12609–12617.
29. Pegoraro E, et al. (2004) Effect of drought on isoprene emission rates from leaves of Quercus virginiana Mill. *Atmos Environ* 38(36):6149–6156.
30. Singsaas EL, Sharkey TD (2000) The effects of high temperature on isoprene synthesis in oak leaves. *Plant Cell Environ* 23(7):751–757.
31. Lebassi B, et al. (2009) Observed 1970–2005 cooling of summer daytime temperatures in coastal California. *J Climate* 22(13):3558–3573.
32. Zhong SY, Whiteman CD, Bian XD (2004) Diurnal evolution of three-dimensional wind and temperature structure in California's Central Valley. *J Appl Meteorol* 43(11):1679–1699.
33. Mearns L, et al. (2009) A regional climate change assessment program for North America. *Eos Trans AGU* 90(36):311.
34. Bloomer BJ, Vinnikov KY, Dickerson RR (2010) Changes in seasonal and diurnal cycles of ozone and temperature in the eastern US. *Atmos Environ* 44:2543–3551.
35. California Air Resources Board (2009) *Ozone Monitoring Concentration Data* (California Air Resources Board, Sacramento).
36. Cox P, Komorniczak A, Weller R (2009) *The California Almanac of Emissions and Air Quality* (California Air Resources Board, Sacramento).
37. Jin SX, Demerjian K (1993) A photochemical box model for urban air-quality study. *Atmos Environ B-Urb* 27(4):371–387.
38. Evans M, Fiore A, Jacob DJ (2003) *The GEOS-Chem Chemical Mechanism, Version 5-07-8* (Harvard University Press, Cambridge, MA).
39. Ito A, Sillman S, Penner JE (2007) Effects of additional nonmethane volatile organic compounds, organic nitrates, and direct emissions of oxygenated organic species on global tropospheric chemistry. *J Geophys Res-Atmos* 112:D063091 10.1029/2005JD006556.
40. Day DA, Wooldridge PJ, Cohen RC (2008) Observations of the effects of temperature on atmospheric HNO3, Sigma ANs, Sigma PNs, and NO_x: Evidence for a temperature-dependent HO_x source. *Atmos Chem Phys* 8(6):1867–1879.
41. Meehl G, al E, eds. (2007) *Global Climate Projections* (Cambridge University Press, Cambridge, UK), pp 747–845.